

Fractography of shear failure surface of softwood decayed by brown-rot fungus

Ryuya Takanashi · Wataru Ishihara · Kei Sawata · Yuzou Sano · Tomonori Azuma · Mitsunori Mori · Akio Koizumi · Yoshihisa Sasaki · Takuro Hirai

Received: 11 November 2013 / Accepted: 5 February 2014 / Published online: 8 March 2014
© The Japan Wood Research Society 2014

Abstract In order to investigate shear failure surface of decayed wood, wood pieces of ezomatsu (*Picea jezoensis*) were exposed to brown-rot fungus (*Fomitopsis palustris*), and standard shear test in radial plane was conducted. The failure surfaces were examined by scanning electron microscopy and surface roughness measurements were also conducted. Transwall failure that the crack elongated parallel to the tracheid axis was observed in the earlywood region through all phases of decay. Intrawall failure principally occurred in the latewood region on the early phase of decay. When decay progressed considerably, transwall failure that the crack elongated perpendicularly to the tracheid axis occurred. And transwall failure was also dominant failure morphology in the latewood region. Fragments of tracheids which were partly peeled out from S₂ layers were observed in some specimens. Size and appearance frequency of fragments of tracheid were smaller and lower when decay progressed. Arithmetic average roughness, which was the index of fragment size and appearance

frequency, had positive correlation to shear strength ratio. Especially, line surface roughness of radial direction, which was measured across the radial files of tracheid, had the highest correlation to the shear strength ratio. The surface roughness would be a good indicator to evaluate the decay degree.

Keywords Scanning electron microscopy · Failure morphology · Average roughness · Shear strength

Introduction

Mechanical properties of wood materials are degraded by brown-rot fungus. Even if a wood material exposed to brown-rot fungus shows little mass loss and change of surface color, its strength often decreases significantly [1, 2]; therefore, studies of wood degradation process in incipient stages of decay caused by brown-rot fungus are needed to understand mechanism of strength deterioration.

Numerous studies that are based on the biological, biochemical and mechanical viewpoints [3–11] have been performed on the wood deterioration by brown-rot fungus. Especially, because the strength deterioration of decayed wood may largely affect safety of timber structures, estimation of degree of deterioration has been performed on partially decayed wood. Methods applied in such studies to date are the pin-penetration depth [5, 6], acoustic emission [7, 8], infrared spectra [9, 10], and X-ray microdensitometry [11]. However, the values obtained by those were influenced by moisture content and distribution of decay. Thus, these methods need non-decayed specimens with same condition. In addition, methods of detection of incipient stages of decay are limited. Detection of the

Part of this study was presented at the 42nd Annual Meeting of the Hokkaido Branch of the Japan Wood Research Society, November 2010, Sapporo, Japan.

R. Takanashi · W. Ishihara · K. Sawata (✉) · Y. Sano · A. Koizumi · Y. Sasaki · T. Hirai
Research Faculty of Agriculture, Hokkaido University,
Sapporo 060-8589, Japan
e-mail: ksawata@for.agr.hokudai.ac.jp

W. Ishihara
Butsurin Corporation, Tokyo 136-8543, Japan

T. Azuma · M. Mori
Forest Products Research Institute, Hokkaido Research
Organization, Asahikawa 071-0198, Japan

decayed part of wood, estimation of decay degree of wood, and evaluation of the residual strength of decayed wood are desired.

Fractography is effective to observe a failure surface and understand failure morphology. For sound wood, Saiki et al. [12] examined tensile failure surfaces. Some studies [13–15] carried out the shear parallel to the grain tests and stated the differences of failure morphology between the earlywood and latewood regions using scanning electron microscopy (SEM) images. Imamura [7] and Furukawa [16] examined tensile broken surface of deteriorated wood. Some observations of tensile failure surface were reported on wood decayed by brown-rot fungus; however, little investigation has been performed on the shear failure surface of wood decayed by the brown-rot fungus.

Therefore, we carried out the shear parallel to the grain tests with wood decayed by a brown-rot fungus, and observation of its shear failure surface by SEM. The relations between failure morphology and the extent of decay were also determined using SEM images. Moreover, besides the microscopic observations, three-dimensional shapes of failure surface were quantitatively evaluated using surface roughness. The deterioration of wood exposed to the brown-rot fungus was estimated by comparing the surface roughness and the shear strength.

Materials and methods

Specimens

The shear parallel to the grain tests were conducted on ezomatsu (*Picea jezoensis*). Eighteen shear specimens [20 (T) × 20 (R) × 30 (L) mm] that had radial shear planes were cut from 4 solid lumbers (A, B, C, and D). The control specimens were also cut from same lumbers. These control specimens were end-matched to each specimen for decay. Table 1 shows the list of specimens.

Decay treatment

To induce decay through a shear plane along grain in the shear specimens, all the surfaces of specimen were coated with epoxy resin first. After epoxy resin hardened, the slit of 1 mm in width and 10 mm in depth was cut in the radial plane (Fig. 1). Then, the specimens were sterilized with ethylene oxide gas and placed in grass bottles containing the brown-rot fungus culture of *Fomitopsis palustris*. Nutrient solution was pure water including 4 % D-glucose, 1.5 % malt extract, and 0.3 % peptone. The exposed specimens were placed in a room kept at constant temperature (24 °C) for period as shown in Table 1. The sterilizing of specimens and decay

treatment were conducted in Forest Products Research Institute, Hokkaido Research Organization, Asahikawa, Japan.

Measurement of shear strength

Shear parallel to the grain tests, block shear tests, according to JISZ2101 [17] were performed on specimens after specimens were conditioned to air-dry humidity control

Table 1 Outline of shear specimens and results of shear tests

Specimen no.	Density (kg/m ³)	$F_{s,c}$ (MPa)	Period of decay (d)	$F_{s,d}$ (MPa)	Failure mode
A1	393	6.45	14	6.47	1
A2	401	7.08	21	5.78	1
A3	458	7.61	21	6.11	1
A4	406	6.11	35	5.45	2
B1	433	8.49	7	7.38	1
B2	456	5.70	7	6.71	1
B3	441	6.22	14	3.79	2
B4	431	7.37	14	5.19	1
B5	438	6.92	21	5.60	1
B6	460	8.47	35	8.84	1
B7	437	5.89	35	5.40	3
C1	383	5.11	7	4.84	2
C2	345	4.27	28	4.35	3
C3	387	4.83	28	4.32	3
C4	333	6.17	56	5.45	3
C5	364	5.26	56	1.28	3
D1	525	7.37	7	7.97	1
D2	522	10.23	14	5.97	3

$F_{s,c}$ Shear strength of the control specimen, $F_{s,d}$ shear strength of the decayed specimen, *Failure mode 1* transwall failure in the earlywood region and intrawall failure in the latewood region. Cracks of the transwall failure in the earlywood region are almost elongated parallel to the tracheid axis, *Failure mode 2* transwall failure in the earlywood region and intrawall failure in the latewood region. Cracks of the transwall failure in the earlywood region are frequently elongated perpendicularly to the tracheid axis, *Failure mode 3* transwall failures in both the earlywood and latewood regions. Cracks of the transwall failure in the earlywood region are frequently elongated perpendicularly to the tracheid axis, and those of the latewood region are elongated both parallel and perpendicularly to the tracheid axis

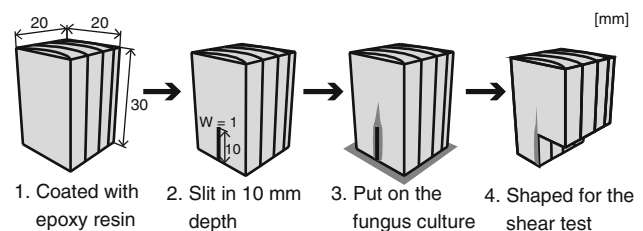


Fig. 1 Dimensions and making procedure of the shear parallel to the grain tests specimen

and shaping the notch. The tests were terminated when the specimens were separated into two blocks. Average moisture content of specimens after shear test and the standard deviation of them were 8.6 and 0.74 %, respectively.

SEM

Small blocks (L:R:T = 6:6:1–2 mm) including shear failure surface were cut from the specimens. The failure surfaces were visually flat in the loaded ends, but heavily rough in the bottom ends as shown in Fig. 2. This may be caused by the grain and the distributions of stress perpendicular to the grain and shear stress along to shear plane [18]. In this study, the blocks for SEM were cut near the notch as shown in Fig. 3. After dried in a desiccator, the blocks were mounted onto specimen stubs for SEM with an electron conductive paste, and then they were coated with platinum by vacuum evaporation. The instrument used for

the SEM was the JSM-6301F (JEOL Ltd.) operated at an accelerating voltage of 2.5 kV.

Surface roughness measurement

After the SEM, the surface roughness of all exposed specimens was measured using laser microscope (VK-9500 KEYENCE Ltd.). The slice samples for the SEM were used in this measurement. This microscope can measure height of a sample surface of 768×1024 pixels. Magnifying power was 10 times and the pitch of measuring surface and height were 1.383 and 0.5 μm , respectively. The measuring area was 1.5 mm^2 and was adjusted to include the earlywood and latewood regions near the edge of notch.

The arithmetic average roughness was adopted as an index of surface roughness in this study. It was calculated by the analysis software (VK-H1A9 KEYENCE Ltd.). The average line surface roughness (R_{aL}) and average plane surface roughness (R_{aA}) were calculated from the variation of height in measuring area as follows:

$$R_{aL} = \frac{1}{l} \int_0^l |f(x)| dx \quad (1)$$

$$R_{aA} = \frac{1}{A} \iint_A |f(x, y)| dx dy \quad (2)$$

where l is measured length, A is measured area, $f(x)$ and $f(x, y)$ are difference between the roughness profile and the average height.

The line surface roughness was defined as the values of the sum of difference between the roughness profile and the average height in the measured range divided by the measured length [19]. Roughness profiles and average line surface roughness of C5 and C3 specimens are shown in Fig. 4 as the example. The high-pass filter that had cutoff value of 0.8 mm was adopted to obtain the roughness profile from the measurement values. The line surface roughness was measured in the longitudinal direction in the earlywood, longitudinal direction in the latewood, and radial direction. The measured lines of the longitudinal direction in the earlywood and latewood were set parallel to a tracheid in the earlywood and latewood regions, respectively. In the case of the radial direction, the measured lines were set across a radial file of tracheids as not including rays. The line surface roughness had a little difference among some measured lines from preliminary tests. Therefore, those measured lines were manually determined. Pair of line surface roughness was obtained from each direction and its average values were used for calculating the roughness

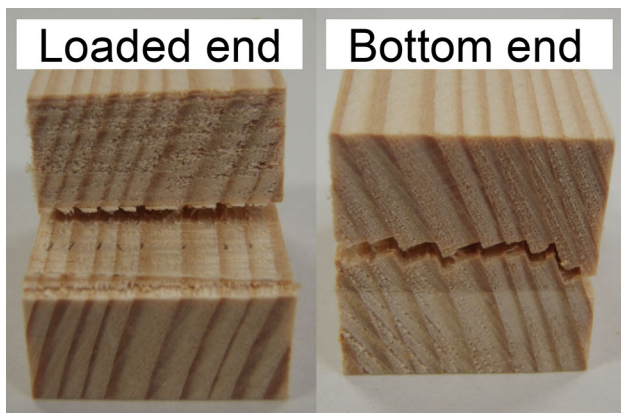


Fig. 2 Shapes of cracking at the loaded side and bottom side of the specimen

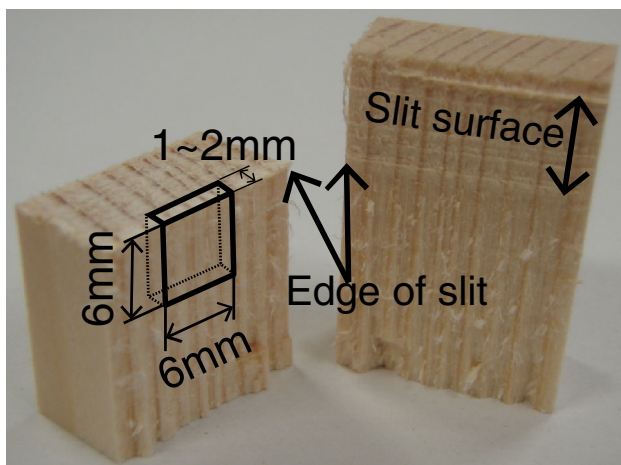
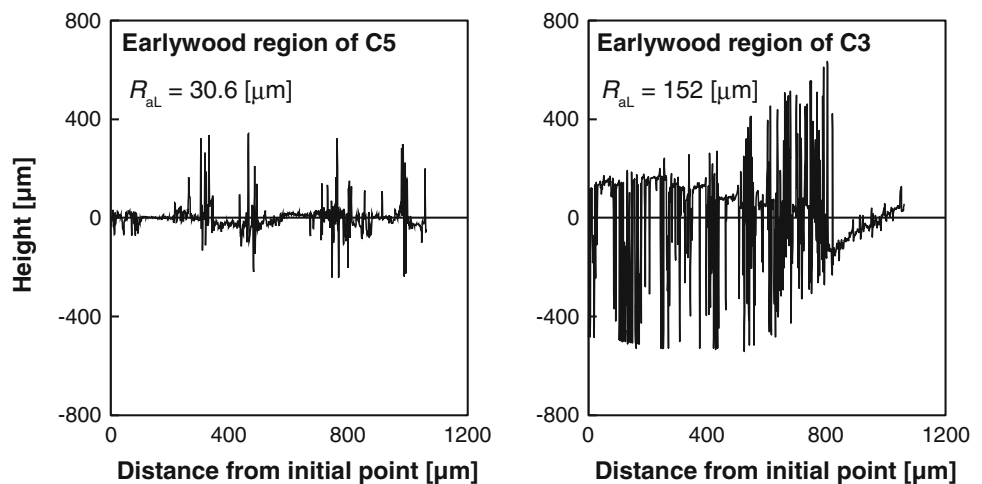


Fig. 3 Sample collection from shear specimen for SEM

Fig. 4 Roughness profiles and average line surface roughness of C5 and C3 specimens. R_{aL} average line surface roughness



index of specimens. The plane surface roughness was expansion of line surface roughness and was calculated from the whole measured area.

Results and discussion

SEM

After the decay treatment and the shear parallel to the grain tests, discoloration due to wood decay was observed on the slit surface and in narrow regions that extended longitudinally from the edge of the slit in the decayed specimens, but no visible damage was observed on the loading and supporting surfaces of the specimens, and all specimens broke at a corner of the notch. The decay procedure of this study proved to be an effective method to investigate the shear strength of decayed wood.

Failure morphology of tracheids was determined from the image of the magnification of 25 times. This image included a 3.6 mm (L) \times 4.9 mm (R) area of a 6 mm \times 6 mm specimen block. And then, the representative failure morphology of tracheids was observed in detail by higher magnification images. Some studies [13–15] that conducted on shear parallel to the grain argued difference of failure morphology between the earlywood and latewood. According to these studies, failure morphology is affected by thickness of the cell wall. In softwood, transwall failure, which is rupture of S_2 secondary cell wall layer resulting in exposure of cell lumina, frequently occurs in earlywood region consisting of thin-walled tracheids. By contrast, intrawall failure predominantly occurs at and around the interface between S_1 and S_2 layers of thick-walled tracheids in latewood region. Because brown-rot fungus decomposes cellulose and degrades cell walls, failure morphology of

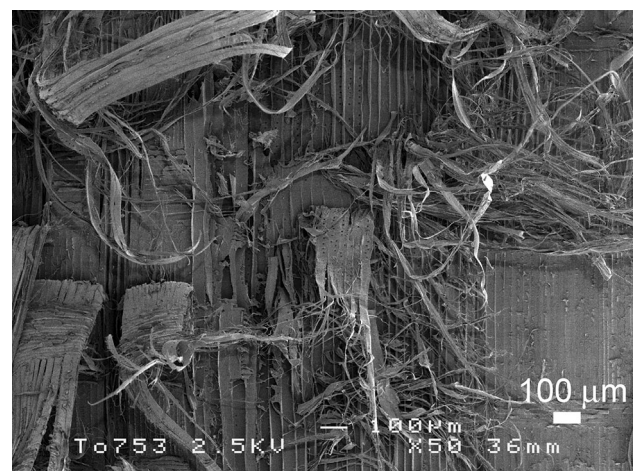


Fig. 5 Shear failure surface of lightly decayed specimen (D1)

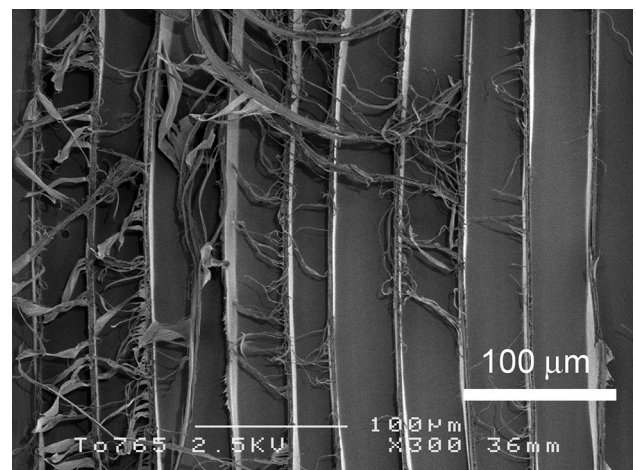


Fig. 6 Enlargement of the earlywood region of D1 specimen showing transwall failure

heavily decayed specimens would be different from that of lightly decayed specimens, and failure morphology of tracheid could be index of decay degree.

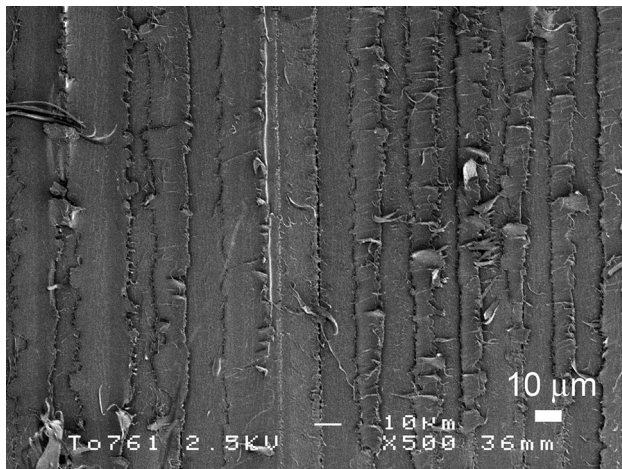


Fig. 7 Enlargement of the latewood region of D1 specimen showing intrawall failure

Figures 5, 6 and 7 show a sheared plane of D1 specimens that were exposed to decay fungus for 7 days (Table 1). The failure morphology was different between the earlywood and latewood regions. The lumina of tracheids are commonly visible as a result of fragment occurrence of transwall failure that extends along cell axis (Fig. 6). By contrast, lumina of tracheids are invisible in the latewood region (Fig. 7). In this case, ruptured layers of tracheid walls can be determined by the microfibril angle (MFA) [15]. On the failure planes of latewood region, MFA was mostly 20° – 30° or 70° – 80° . This indicates that the intrawall failure in latewood tracheids occurred at and around boundaries between S_1 and S_2 . These features in failure morphology found in slightly decayed woods are similar to failure morphology reported for sound wood [13, 15].

Figure 8 shows a sheared plane of B3 specimen which was exposed to decay fungus for 14 days (Table 1). The failure morphology of B3 specimen resembles that of D1 specimen; however, some tracheids were cut off perpendicularly to the grain in the earlywood region. These failures are also classified under transwall failure; however, the orientation of failure differs from the case of slightly decayed specimens. Thus, transwall failure that the crack elongates perpendicularly to the tracheid axis is distinguished from transwall failure that the crack elongates parallel to the tracheid axis. Figure 9 shows sheared planes of C3 specimen which was exposed to decay fungus for 28 days (Table 1). Transwall failure commonly occurred in not only earlywood but also latewood regions. Failure morphology in the latewood region should be changed as cell walls of tracheids become thin. Moreover, many transwall failures perpendicular to the tracheid axis in the earlywood region were present in this failure morphology. The frequency of existence of transwall failure perpendicular to the tracheid axis in the earlywood region and

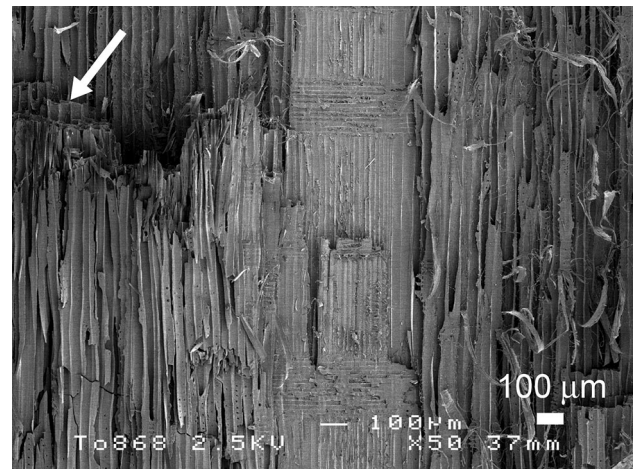


Fig. 8 Shear failure surface of B3 specimen. Arrow indicates transwall failure that the crack elongated perpendicularly to the tracheid axis

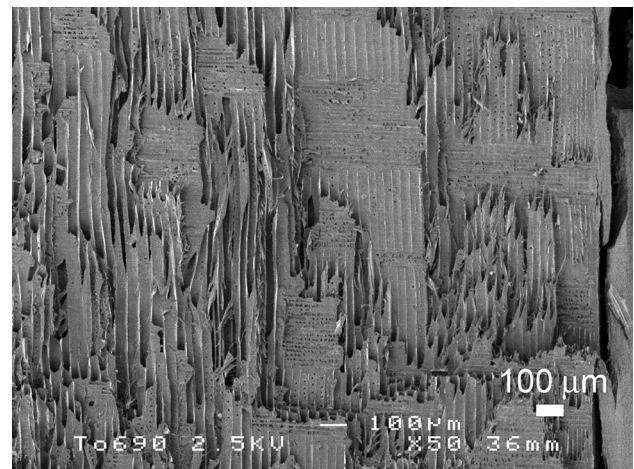


Fig. 9 Shear failure surface of considerable decayed specimen (C3)

transwall failure in the latewood region would be features of decay degree.

From the results described above, failure morphology was classified into 3 modes (Fig. 10). Mode 1 was transwall and intrawall failures in the earlywood and latewood regions, respectively. Transwall failures parallel to the tracheid axis were dominant in this mode. Mode 2 was also transwall and intrawall failures in the earlywood and latewood regions, respectively. A characteristic of the transwall failures, which is not dominant in mode 1, is that the crack elongated perpendicularly to the tracheid axis. When such failures were observed in the majority of the image of the magnification of 25 times, the failure morphology was decided to mode 2. Mode 3 was transwall failure in both the earlywood and latewood regions. When transwall failures were observed in the majority of latewood region,

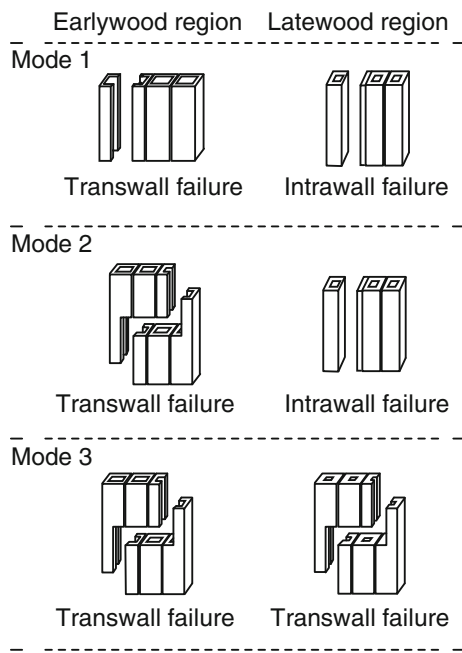


Fig. 10 Failure modes

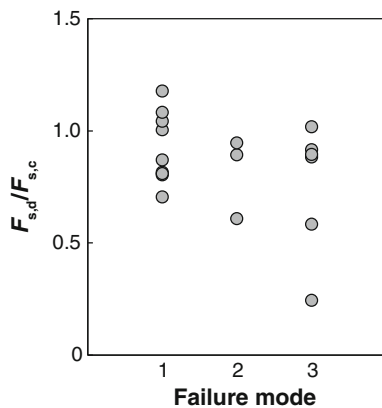


Fig. 11 Relations between the ratio of shear strength of decayed specimen to that of control specimen and failure modes. Failure modes 1–3: see Table 1 and Fig. 10. $F_{s,c}$ shear strength of the control specimen, $F_{s,d}$ shear strength of the decayed specimen

the failure mode was decided to mode 3. The characteristics of mode 3 was that the tracheid in the latewood region was cut both parallel and perpendicular to the tracheid axis and the transwall failures perpendicular to the tracheid axis were also dominant in the earlywood region. The transition of failure morphology proceeded continuously with an extent of decay.

The shear strength and the failure modes of all specimens are shown in Table 1. Figure 11 shows the relations between the ratio of shear strength of decayed specimen to that of control specimen and failure modes. Because wood strength has variation, shear strength of specimen with little

or a little degradation may be larger than that of end-matched control specimen. Four specimens with failure mode 1 and one specimen with failure mode 3 had the shear strength ratio of 1.0 or more. The former would be little degraded by decay. Although the latter was observed the transwall failures in the latewood region, the partial degradation would little cause the shear strength loss. Some of specimens that had failure modes 2 and 3 showed small shear strength ratio and significant strength loss was observed in a specimen with failure mode 3. Specimens with large strength loss exhibited different failure morphologies in comparison to the others.

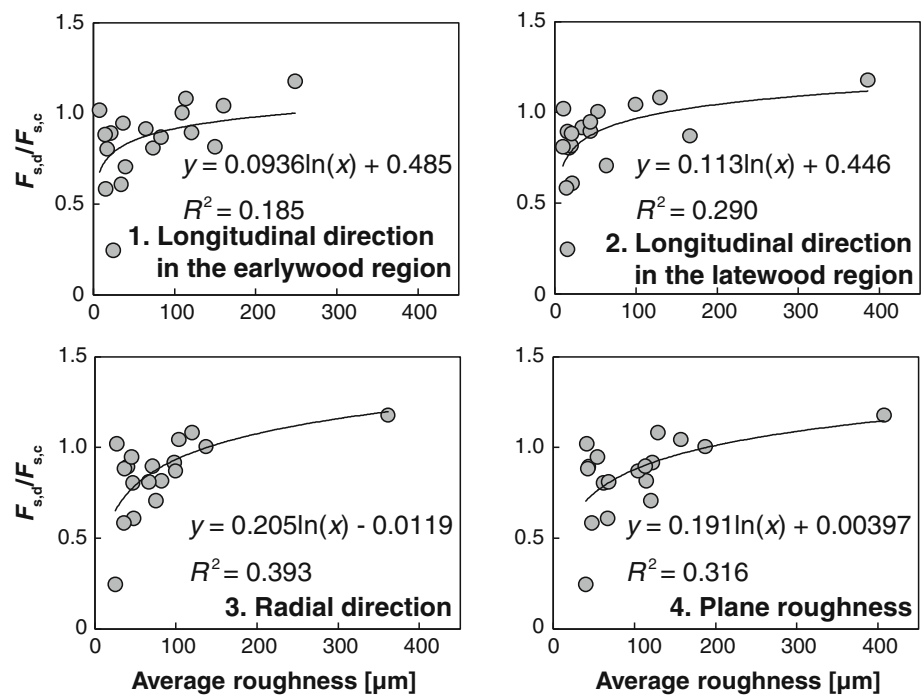
On sheared plane of sound wood, peeling out of secondary wall of tracheid has been observed, called “flags” by Côté and Hanna [13]. The peeling out of tracheid is usually observed in the earlywood region. The peeling out of tracheid was observed in the specimen with high shear strength in this study (Fig. 5). As shear strength was decreased, size of fragment of tracheid seemed to be smaller and its appearance frequency of fragment seemed to be lower. In addition, specimens with considerable small shear strength showed no fragment of tracheid caused by peeling out (Fig. 9). The size and appearance frequency of fragment of tracheid may depend on the extent of decay. The extent of decay, which includes incipient decay to significant decay, could be evaluated by investigation of fragment of tracheid. Therefore, the shape of failure surface was quantitatively evaluated by the surface roughness.

Surface roughness measurements

The size and appearance frequency of fragment of tracheid affected the roughness profile of failure surface. As shown in Fig. 4, the C3 specimen which had little strength loss showed significantly ragged surface while the roughness profile of the C5 specimen which showed large strength loss exhibited small variation. This study conducted the calculation of 4 kinds of the arithmetic average roughness: the line surface roughness in the longitudinal direction in the earlywood, longitudinal direction in the latewood and radial direction, and the plane surface roughness. Figure 12 shows the relations between the ratio of shear strength of decayed specimen to that of control specimens and average roughness, including regression formulas of the logarithm. Regardless of kind of average roughness, the shear strength tended to decrease with decreasing the average roughness. The relations between the strength ratio and the line surface roughness in the radial direction showed the highest correlation of the 4 kind of surface roughness.

From the results described above, the fragments of tracheid caused by peeling out might be reliable index to evaluate strength loss. The line surface roughness in the radial direction was better appropriate index to estimate the

Fig. 12 Relations between the ratio of shear strength of decayed specimen to that of control specimen and arithmetic average roughness. $F_{s,c}$ shear strength of the control specimen, $F_{s,d}$ shear strength of the decayed specimen



degree of decay. In addition, measured lines were designed manually in this study, thus, the relative simple measurement method, for example only one line measuring, can be effective to detect degree of decay.

The results of observation by SEM and measurement of surface roughness showed that size of fragment of tracheid was smaller and its appearance frequency of fragment was lower as decay progressed. It is known that brown-rot fungus decomposes cellulose chain [3]. Change of surface roughness of the failure plane might show qualitative change of cell wall by decay. Reduction in size and appearance frequency of fragment of tracheid might be evidence of decomposition of cellulose chain of cell wall by decay.

Conclusions

Tests of shear parallel to the grain in radial plane and fractography of the shear failure surface were conducted for ezomatsu exposed to the brown-rot fungus. The results obtained can be summarized as follows:

1. Transwall failure that the crack elongated parallel to the tracheid axis occurred in the earlywood region irrespective of degree of decay.
2. Transwall failure that the crack elongated perpendicularly to the tracheid axis occurred when wood was decayed significantly.
3. Intrawall failure was dominant failure morphology in the latewood region in incipient stages of decay. When decay progressed considerably, the failure morphology

in the latewood region changed from intrawall failure to transwall failure.

4. Size and appearance frequency of fragment of tracheid caused by peeling out were dependent on degree of decay. As decay progressed, size of fragment of tracheid was smaller and appearance frequency of fragment of tracheid was lower.
5. There was a positive correlation between shear strength ratio and average roughness of shear failure surface. Line surface roughness in the radial direction could be a reliable indicator to estimate strength loss.

Acknowledgments The authors gratefully acknowledge support in the laser microscopic measurement by Prof. Yasumitsu Uraki and Ms. Yuka Tasaki, and SEM photographing by Dr. Masanori Yasui.

References

1. Richards DB (1954) Physical changes in decaying wood. J Forest 52:260–265
2. Takahashi M, Nishimoto K (1967) Studies on the mechanism of wood decay (I): changes in strengths of BUNA and SUGI wood as decay proceeds (in Japanese). Wood Res 41:75–89
3. Kleman-Leyer K, Agosin E, Conner AH, Kirk TK (1992) Changes in molecular size distribution of cellulose during attack by white rot and brown rot fungi. Appl Environ Microbiol 58:1266–1270
4. Munir E, Yoon JJ, Tokimatsu T, Hattori T, Shimada M (2001) A physiological role for oxalic acid biosynthesis in the wood-rotting basidiomycete *Fomitopsis palustris*. Proc Natl Acad Sci USA 98:11126–11130

5. Thaler N, Lesar B, Humar M (2012) Correlation between brown rot decay and Pilodyn measurements. *Eur J Wood Prod* 70:893–895
6. Toda M, Mori M, Ohashi Y, Hirai T (2010) Effect of wood decay on the shear performance of nailed timber joint (in Japanese). *Mokuzai Gakkaishi* 56:41–47
7. Imamura Y (1990) Detection of decay and termite attack in wood using AE monitoring (in Japanese). *Wood Res Tech Notes* 26:38–60
8. Raczkowski J, Lutomski K, Moliński W, Woś R (1999) Detection of early stages of wood decay by acoustic emission technique. *Wood Sci Technol* 33:353–358
9. Green B, Jones PD, Nicholas DD, Schimleck LR, Shumulsky R (2011) Non-destructive assessment of *Pinus* spp. wafers subjected to *Gloeophyllum trabeum* in soil block decay tests by diffuse reflectance near infrared spectroscopy. *Wood Sci Technol* 45:583–595
10. Takahashi M, Nishimoto K (1967) Studies on the mechanism of wood decay (2): changes in infrared spectra of BUNA and SUGI wood as decay proceeds. *Wood Res* 42:1–12
11. Macchioni N, Palanti S, Rozenberg P (2007) Measurements of fungal wood decay on Scots pine and beech by means of X-ray microdensitometry. *Wood Sci Technol* 41:417–426
12. Saiki H, Furukawa I, Harada H (1972) An observation on tensile fracture of wood by scanning electron microscope (in Japanese). *Bull Kyoto Univ For* 43:309–319
13. Côté WA, Hanna RB (1983) Ultrastructural characteristics of wood fracture surfaces. *Wood Fiber Sci* 15:135–163
14. Müller U, Sretenovic A, Gindl W, Grabner M, Wimmer R, Teischinger A (2004) Effects of macro- and micro-structural variability on the shear behavior of softwood. *IAWA J* 25:231–243
15. Gindl W, Teischinger A (2003) Comparison of the TL-shear strength of normal and compression wood of European larch. *Holzforschung* 57:421–426
16. Furukawa I (1988) Studies on safety in timbers and woody materials (I): fractographic approach to evaluating the brashness of wood (in Japanese). *Res bull Tottori Univ For* 17:151–169
17. JIS Z 2101 (2009) Methods of test for wood (in Japanese). Japanese Industrial Standard Association, Tokyo
18. Okusa K (1980) Studies on the shearing of wood: especially on the elastic-plastic theory and fracture mechanics: III. On the stress singularity and the energy release rate in the chair-type (JIS) shearing specimen (in Japanese). *Bull Fac Agric Kagoshima Univ* 30:201–215
19. JIS B 0601 (1994) Surface roughness—Definitions and designation (in Japanese). Japanese Industrial Standard Association, Tokyo